Acta metall. Vol. 35, No. 11, pp. 2701–2710, 1987
Printed in Great Britain.

0001-6160/87 $3.00 + 0.00

MICROCRACK TOUGHENING IN ALUMINA/ZIRCONIA

M. RÜHLE,† A. G. EVANS, R. M. McMEEKING and P. G. CHARALAMBIDES
Materials Program, University of California, Santa Barbara, CA 93106, U.S.A.

and

J. W. HUTCHINSON

Division of Applied Sciences, Harvard University, Cambridge, MA 02139, U.S.A.

(*Received* 14 *February* 1987)

Abstract—Analysis of microcrack toughening in Al_2O_3/ZrO_2 is presented. The study consists of *experimental* measurements of the microcrack parameters that dictate the predicted level of toughening, as well as *calculations* of the toughness using microcrack models based on the microcracks *observed* in the process zone. An effective comparison between theory and experiment is thereby achieved. The comparison reveals moderate agreement, but also establishes that several aspects of microcrack toughening are not yet sufficiently developed to allow prediction of trends in toughness with microstructure.

Résumé—Nous présentons l'analyse du durcissement des microfissures dans Al_2O_3/ZrO_2. L'étude comprend des mesures *expérimentales* des paramètres des microfissures qui contrôlent le niveau prédit de durcissement, ainsi que des *calculs* de durcissement à partir de modèles de microfissures basés sur les microfissures *observées* dans la zone étudiée. Nous comparons donc réellement la théorie et l'expérience. Cette comparaison révèle un accord moyen, mais elle montre également que plusieurs aspects du durcissement des microfissures ne sont pas encore assez développés pour qu'on puisse prédire les variations de la dureté avec la microstructure.

Zusammenfassung—Die Zähigkeitsverbesserung durch Mikrorisse wird in Al_2O_3/ZrO_2 analysiert. Die Untersuchung zieht *experimentelle* Messungen der Parameter der Mikrorisse, die die vorausgesagte Höhe der Zähigkeit bestimmen, heran und benutzt *Berechnungen* der Zähigkeit, die mit Mikrorißmodellen auf der Basis der in der Prozeßzone *beobachteten* Mikrorisse durchgeführt werden. Dadurch können Theorie und Experiment wirksam miteinander verglichen. Aus diesem Vergleich folgt eine mäßige Übereinstimmung; er zeigt jedoch auch, daß einige Aspekte der Zähigkeitverbesserung durch Mikrorisse noch nicht genügend entwickelt worden sind, um die Tendenzen der Zahigkeit in Abhängigkeit von der Mikrostruktur vorhersagen zu können.

1. INTRODUCTION

The toughening of ceramics by a microcrack process zone has been extensively speculated upon in the literature [1–3]. The most recent and comprehensive approach [4–6] establishes considerable similarities between transformation and microcrack toughening, by relating the change in toughness to the permanent dilatation and the reduced modulus of the material in the process zone. In microcracking materials, the requisite dilatation arises because the microcracks relieve local residual tensile stresses, caused by thermal expansion mismatch [4, 5], transformation [7] etc. Despite the extensive theoretical research on the subject of microcrack toughening, there have been no systematic experimental studies that attempt to provide the basis for a direct comparison between theory and experiment. The purpose of the present study is to provide a closely coupled experimental and theoretical investigation of this phenomenon.

Recent studies on zirconia toughened alumina [8] (ZTA) suggest that this material is an ideal candidate for such a systematic investigation. Specifically, in this material, there is a minimal effect on toughness of the ratio of monoclinic to tetragonal ZrO_2 (Fig. 1), implying that transformations and microcracking have similar toughening potency. Furthermore, transmission electron microscopy studies have revealed the existence of a microcrack process zone in ZTA containing predominantly m-ZrO_2. Present logic thus suggests that macrocrack propagation provides the additional stress needed to initiate microcracks at thermally-transformed (but uncracked) monoclinic particles.

The microcrack toughening models [4–6] indicate that the toughening should relate to such quantities as: the number density of microcracks in the process zone, the microcrack length distribution and the residual opening of the microcracks. Measurements of these quantities are afforded primary attention in the experimental component of the present research. Thereafter, the toughening pertinent to the microcrack morphologies observed in the process zone is

†Formerly with the MPI für Metallforschung, Stuttgart, F.R.G.

predicted, using established procedures [6, 7]. The comparison between theory and experiment then provides the requisite assessment of the potency of the microcrack toughening process.

2. EXPERIMENTAL

2.1. General features

The present microstructural studies were performed on various ZTA materials [8]. Each material studied contained 15 vol.% ZrO_2. However, by utilizing different processing procedures the proportion of ZrO_2 thermally transformed to the monoclinic phase was varied between 14 and 77% (Fig. 1).

Transmission electron microscopy (TEM) studies have revealed that all ZrO_2 particles and Al_2O_3 grains in these materials are facetted and that the ZrO_2 particles are intercrystalline. The size distribution of the grains and particles have been measured from the projected areas, A, by estimating the radii, b, in accordance with $2b \approx \sqrt{A}$ [9]. The direct estimation of the size distribution from the projected area is clearly applicable only when the foil thickness exceeds the effective radius of the largest microstructural feature. Consequently, foils up to 0.8 μm in thickness have been used for this analysis, to ensure incorporation of the majority of particles (Table 1). The radii determined in this manner were separated into different nonlinear size groups [9] (Table 1). The

Table 1. Particle radius range (in μm) of the different size groups—logarithmic scale

Size group	Lower bound	Upper bound
1	0	0.05
2	0.05	0.07
3	0.07	0.09
4	0.09	0.12
5	0.12	0.16
6	0.16	0.22
7	0.22	0.30
8	0.30	0.40
9	0.40	0.50
10	0.50	0.71
11	0.71	0.96
12	0.96	—

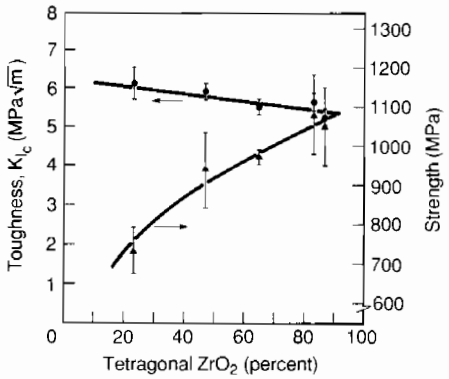

Fig. 1. Trends in the strength and toughness of ZTA with relative tetragonal content for a 15 vol. % ZrO_2 material.

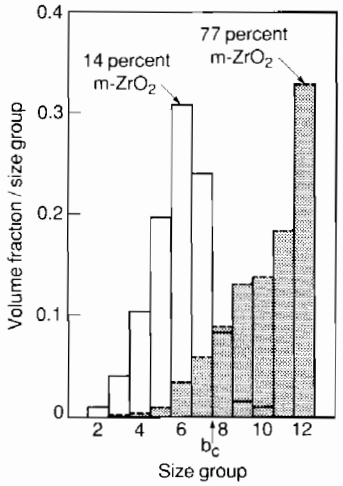

Fig. 2. ZrO_2 particle size distribution for the materials having 14 and 77% of the ZrO_2 in the monoclinic form. The size groups are defined in Table 1. All particles larger than b_c are monoclinic.

resultant ZrO_2 particle size distributions are summarized in Fig. 2, using the *volume* fraction per size group as the ordinate. In accordance with previous studies, ZrO_2 particles with radius $b_c > 0.3$ μm were found to be monoclinic, and contained twin lamellae.

All grains (Al_2O_3 and ZrO_2) were determined to be circumvented by a continuous amorphous grain boundary film, as revealed by dark field TEM [11] (Fig. 3). Additionally, small interfacial microcracks were usually observed between monoclinic ZrO_2 par-

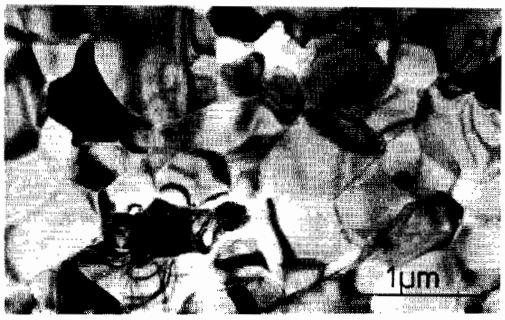

(a)

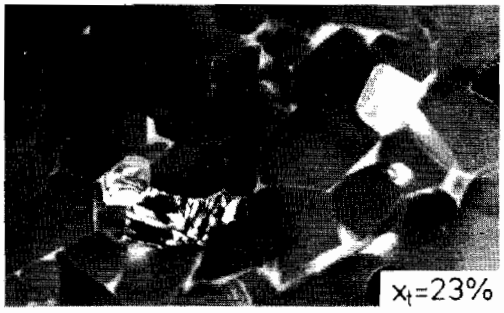

(b)

Fig. 3. TEM micrographs indicating the continuous amorphous grain boundary phase. (a) Bright field image, (b) dark field image: the bright lines at the grain boundaries are indicative of an amorphous grain boundary phase [11].

Fig. 4. Three examples of microcracks observed at twin terminations in the Al_2O_3/ZrO_2 interface.

ticles and the Al_2O_3 matrix grains in those regions where the twin planes of m-ZrO_2 terminated (Fig. 4). Occasional, thermally-induced microcracks were also detected, *remote* from the macrocrack (Fig. 5). These were invariably associated with larger monoclinic ZrO_2 particles: the largest having a diameter of $\sim 7\,\mu m$. These cracks are believed to dominate the strength, resulting in strength less than those apparent in the predominantly tetragonal material (Fig. 1).

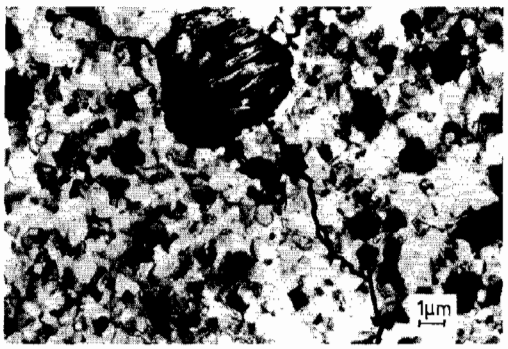

Fig. 5. A TEM revealing a thermally induced microcrack at a large thermally transformed monoclinic ZrO_2 particle.

2.2. *Microcracks*

Matrix microcracking caused by the growth of macrocracks was studied by introducing steady state macrocracks and preparing thin foils at four distances, y, from the macrocrack plane (0.5, 1.5, 3 and $6\,\mu m$). The preparation of such foils required the development of a special thinning procedure. Specifically, a cylinder was cut normal to the macrocrack surface. A prescribed layer (0.5, 1.5, 3 or $6\,\mu m$) was then sputtered from the crack surface by calibrated ion-thinning. Finally, back thinning generated the thin TEM specimen located at the requisite distance from the crack plane.

Radial matrix microcracks were observed, as exemplified in Fig. 6. All such radial microcracks occurred along grain boundaries in the Al_2O_3. Usually, the interface between the Al_2O_3 and ZrO_2 was debonded at the origin of the microcrack (Fig. 7).

The detectability of radial microcracks depends sensitively on their inclination with respect to the incoming electron beam. In particular, the visibility decreases strongly and the characteristic defocus changes drastically when an overlap occurs with the projection of the flanks of the microcrack. This condition develops when the inclination angle between the flanks of the microcrack and the incoming electron beam exceeds, $\tan^{-1}(\delta/c)$, where δ represents the residual opening and c the length of the micro-

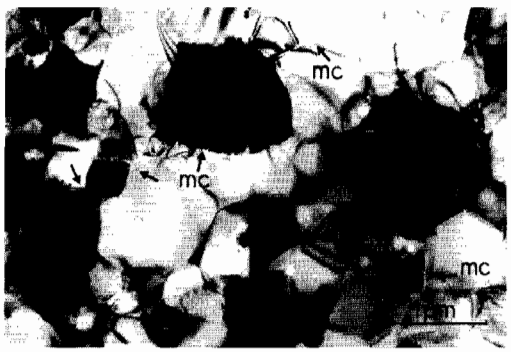

Fig. 6. A TEM micrograph revealing a typical microcrack in the process zone.

Fig. 7. A TEM micrograph showing the debonding of the interface near a microcrack.

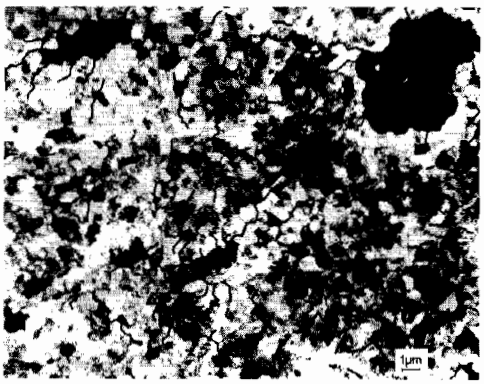

Fig. 9. A TEM micrograph with all observable microcracks marked.

crack.† Trends in the visibility of microcracks upon tilting around *one* axis (Fig. 8) indicate that, in essence, because δ/c is small, tilting in all directions would be needed to detect each microcrack present in the foil. However, tilting in the TEM is limited to $\pm 45°$ in all directions so that only 0.3 of the solid angle is covered. Therefore, the fraction of detectable microcracks is limited to ~ 0.3.

Subject to this detectability limitation large regions of TEM foils of known thickness have been investigated. One example is shown in Fig. 9, wherein all microcracks observable under different tilting conditions are marked. It is noted, on average, that at least 2 microcracks emanate from each m-ZrO_2 particle. In most cases, the microcracks terminate at the Al_2O_3 grain triple junctions. The associated projected length, l, of each microcrack was measured and related to the radius, b, of the originating monoclinic ZrO_2 particle (Fig. 10). Additionally, the residual opening of the microcracks, δ was determined at the ZrO_2 particle intersection, where the opening is usually largest (Fig. 11).

†In cases where the microcrack extends completely through the TEM foil, c corresponds with the foil thickness t.

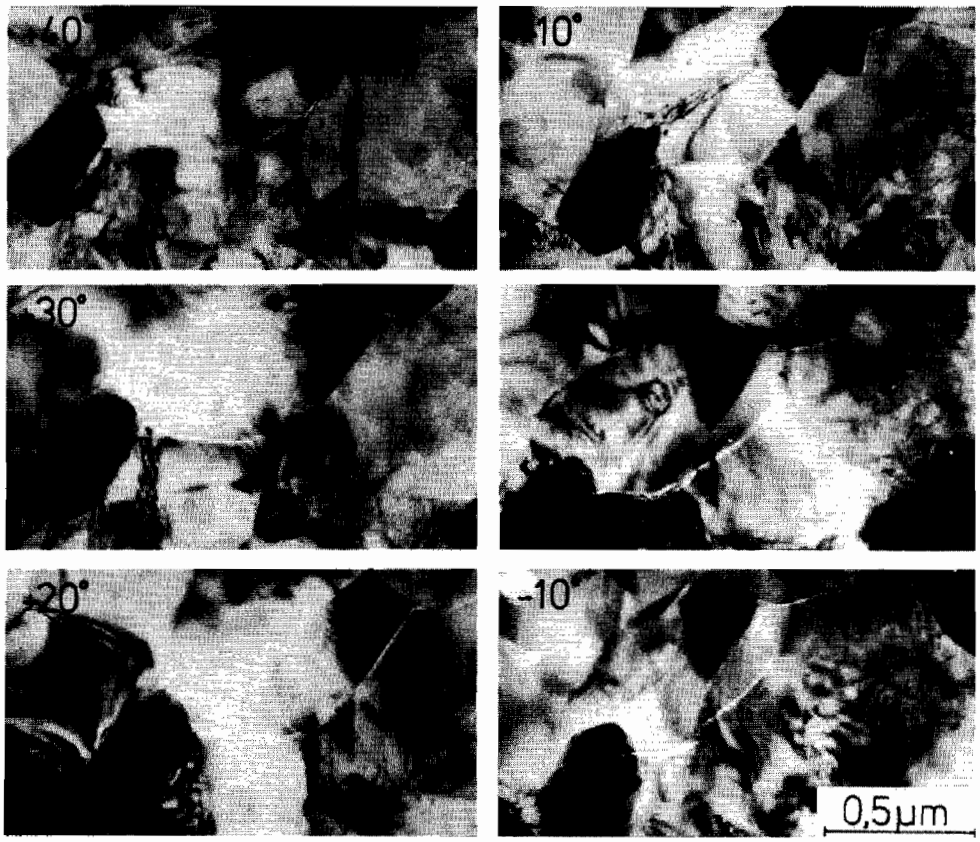

Fig. 8. A tilting sequence indicating the technique used to trace microcracks.

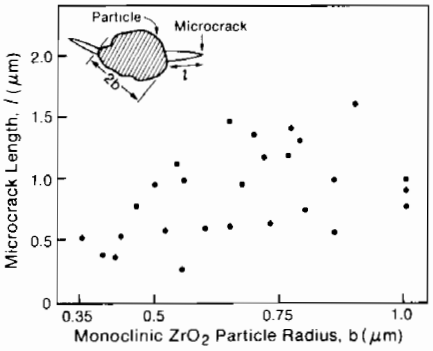

Fig. 10. Trends in microcrack length, l, with the effective radius, b, of the associated monoclinic ZrO_2 particles.

The utility of microcrack length measurements is facilitated by defining a representative geometry and determining the related microcrack density parameter [12].

$$\epsilon = N\langle c^3 \rangle \tag{1}$$

where N is the number of microcracks per unit volume and c is the relevant microcrack dimension. Evaluation of the microcrack profiles observed by tilting suggests that each ZrO_2 particle is circumvented by a radial microcrack [Fig. 12(a)], consistent with the symmetry of the residual strain field around each particle. The model depicted in Fig. 12(b) is thus used for further analysis.

A number of difficulties exist regarding evaluation of ϵ from TEM foils primarily because applicable foil thickness ($\lesssim 0.8\,\mu$m) provide only limited sections through the microcrack/particle configuration (Fig. 13). Sections that intercept the microcrack, but not the particle (Section II in Fig. 13), would not reveal the microcrack, because removal of the initiating particle eliminates the residual opening. Furthermore, sections that intercept only a small segment of the particle (Section III in Fig. 13) are also subject to appreciable relief of the residual opening and hence, exhibit restricted microcrack detectability. Consequently, the analysis of microcrack densities is essentially limited to sections that intercept the particle at both surfaces of the foil (Section I in Fig. 13). For very thin foils, Fig. 13 indicates that the detected fraction should be $\sim b/(b+c)$. Hence, studies performed on foils ranging in thickness between 0.1 and 0.8 μm have been used to examine sectioning related detectability.

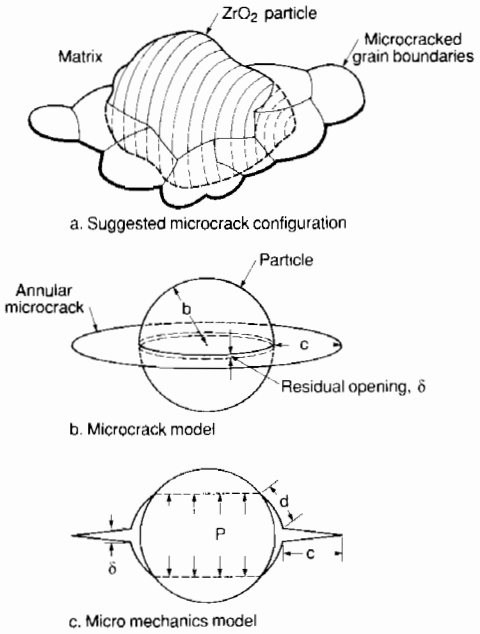

Fig. 12. The microcrack model used to measure crack densities and to analyze the changes in crack volume and elastic modulus: (a) a schematic drawing of a typical configuration; (b) the microcrack model used for analysis; (c) the mechanics model.

An example of the frequency distribution, $f(l)\,\mathrm{d}l$, of projected microcrack lengths, (governed by the above restrictions) measured on a series of TEM foils from the material containing 77% m-ZrO_2 is plotted in Fig. 14. The microcrack density may be evaluated from such a frequency distribution by using a procedure devised by Budiansky and O'Connell [12],

$$\epsilon = (6/\pi)\int_0^\infty l^2 f(l)\,\mathrm{d}l/q \tag{2}$$

where q is the fraction of microcracks detected. The results obtained are plotted in Fig. 15 recalling that two traces constitute one annular crack (Fig. 13).

Several features are evident from Fig. 15. The microcrack density diminishes with distance from the

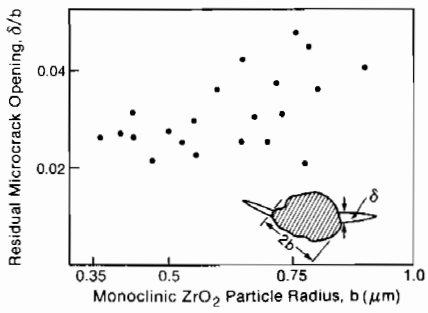

Fig. 11. Trends in residual crack opening with particle size.

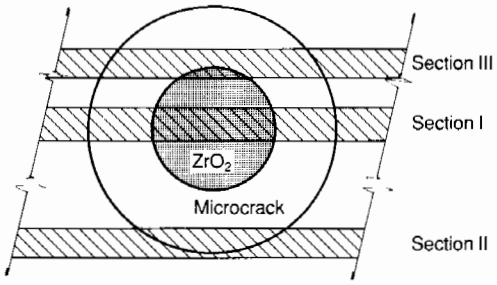

Fig. 13. Typical thin foil sections through microcracked particles. Only microcracks intercepted by sections of type I are consistently detected.

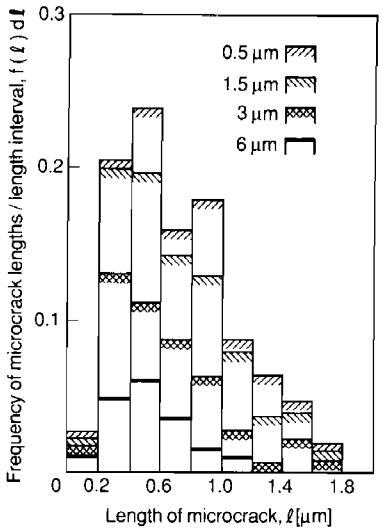

Fig. 14. The microcrack length distributions at four distances (0.5, 1.5, 3 and 6 μm) from the crack plane obtained on a material containing 77% initial m-ZrO_2. Note the position insensitivity.

crack plane. A maximum density ϵ_s adjacent to the crack surface suggests a saturation value, governed by the total ZrO_2 particle content. The decrease with distance y is approximately linear, such that

$$\epsilon \approx \epsilon_s(1 - y/h) \tag{4}$$

where h is the process zone width.

3. SOME BASIC THEORETICAL RESULTS

The changes in toughness imparted by a microcrack process zone [4, 6, 13] are based on determinations of the volume increase, ΔV, provided by the residual opening of the cracks and changes in elastic properties. The dilatation and modulus reduction can then be incorporated into expressions for the microcrack toughening [4, 6, 13]. The magnitudes of the dilatation and of the modulus reduction depend both on microcrack geometry and the stress-free strain caused by thermal transformation and thermal expansion mismatch, as discussed in detail elsewhere [6, 7]. The results presented in this section are specialized to the predominant microcrack geometry inferred from the present observations on ZTA, [Fig. 12(b)] and expressed in terms of the characteristic dimensions c and $\xi = c/b$ [Fig. 12(b)], as well as the residual opening, δ, of the representative annular microcrack.

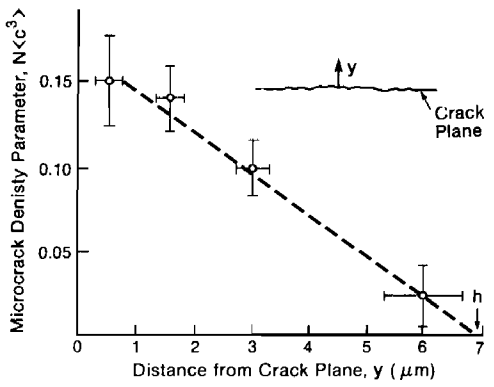

Fig. 15. Trends in the microcrack density parameter, $\epsilon = N\langle c^3\rangle$, with distance y from the crack surface.

Analysis of the residual *dilatation* caused by the microcracks commences with a determination of the crack opening displacements, governed by the traction distribution depicted in Fig. 12(c). The analysis reveals (Appendix) that the microcrack opening is almost triangular, except near the tip, consistent with the microcrack observations (Fig. 7). The volume ΔV between the crack surfaces can then be derived as (Appendix)

$$\Delta V/b^2\delta \approx 3.6\xi. \tag{5}$$

The dilatation, $\theta \equiv N\Delta V$, is thus

$$\theta = g(\xi)(\delta/b)\epsilon \tag{6}$$

where

$$g(\xi) \equiv 3.6\xi^{-2}.$$

The *modulus* change can be deduced using the method of Budiansky and O'Connell [12] utilizing the strain energy removed upon formation of the microcrack. For annular microcracks having the geometry depicted in Fig. 12(b) the reduced shear modulus, $\bar{\mu}$, of the composite is derived as (Appendix)

$$1 - \bar{\mu}/\mu = (16/9)\epsilon(1 + 2\xi^{-1})^{3/2}$$
$$\left[1 - \frac{6.8[(\xi^2 + 2\xi)^{1/2} - \xi]/(\xi + 2)}{\pi(\bar{\mu}/\mu)(d/b) + 4[(\xi^2 + 2\xi)^{1/2} - \xi]}\right]$$
$$\equiv \epsilon H(\xi, \bar{\mu}/\mu_p, d/b) \tag{7}$$

where μ_p is the shear modulus of the ZrO_2 particle, and d is the extent of crack growth along the interface [Fig. 12(c)]. For the modulus ratio pertinent to ZTA, $\mu/\mu_p \approx 2$, $d/b \cong 1$ (Appendix), and for ξ characteristic of the present material ($\xi \approx 1.4$, Fig. 10), $H \approx 5.8 - 8\xi$.

The change in *toughness* caused by crack shielding from a microcrack process zone is expressible in terms either of the J-integral or the stress intensity factor K, depending upon the criterion for crack extension. The use of K is deemed most appropriate when the microcrack density exhibits saturation near the crack tip [4, 6, 13]. Consequently, since the present results for ZTA exhibit a tendency toward saturation (Fig. 15), the solutions provided by the appropriate K analysis are used for purposes of further consideration. However, this choice is not critical to the subsequent comparisons between experiment and theory. At lowest order, for small scale microcracking, the shielding contribution from the modulus reduction and from the dilatation can be regarded as independent and additive. The steady-state dilatation shielding ΔK_d for sub-critical micro-

cracking when $\theta \to 0$ at $y = h$ is given explicitly by [7]

$$\Delta K_d = -\frac{\lambda(1+\nu)\mu}{(1-\nu)} \int_0^{\theta(0)} \sqrt{y(\theta)}\, d\theta \qquad (8)$$

where y is the distance from the crack plane and λ is a coefficient that depends on the constitutive law that characterizes the microcracking process. For physically reasonable laws, λ ranges between ~ 0.4 and 1.0 [7]. The former obtains for microcracking controlled by the mean stress, while the latter applies when microcrack nucleation is dictated by the maximum principal tension. The appropriate choice must be consistent with the microcrack observations.

The steady-state shielding induced by modulus reduction, ΔK_m, is independent of the size of the process zone, h [4, 6], but has some dependence on zone shape and on the form of the constitutive law that governs microcracking. A close approximation suitable for initial purposes is [6];

$$\frac{\Delta K_m}{K} = [(k_1 - 5/8)(\mu/\bar{\mu} - 1) + (k_2 + 3/4)(\bar{\nu}\mu/\bar{\mu} - \nu)](1-\nu)^{-1} \qquad (9)$$

where $k_1 \sim 0.017$ and $k_2 \approx -0.043$, as appropriate for microcracks generated by a critical mean stress, and K refers to the *composite*. Deviations from additivity of ΔK_m and ΔK_d occur when these quantities exceed ~ 0.2 K and when interaction effects cause changes in zone shape [13].

4. COMPARISON BETWEEN THEORY AND EXPERIMENT

The initial basis for the comparison between theory and experiment centers upon the measurements of microcrack length and orientation. As revealed in Section 2, these measurements indicate that the microcracks have essentially random orientation at all locations with respect to the crack plane and that the microcrack lengths have no systematic dependence on the distance from the crack plane. These measurements have several implications. The invariance and randomness indicate that microcracking is dominated by the initial residual field around the particles, even close to the crack plane, suggestive of relatively low stresses everywhere *within* the process zone. Such behavior is consistent with substantial microcrack degradation of the tip toughness as elaborated below. The orientation randomness also suggests that the contribution of the residual strain field to toughness is dictated by the dilatational component.

The *residual strain* contribution to the *shielding* can be deduced from equation (4), (6) and (8) as

$$\Delta K_d \approx -(2/3)(1+\nu)\lambda\mu \times (\delta/b) g(\xi) \epsilon_s \sqrt{h}(1-\nu)^{-1} \qquad (10)$$

with ξ being the average value obtained from Fig. 10. The appropriate values of the parameters in equation (10) are: $\xi \approx 1.4$ giving $g = 1.84$, $\delta/b \approx 0.03$ (Fig. 11), $\mu \approx 150$ GPa, $\epsilon_s \approx 0.15$ (Fig. 15). Consequently, for the material containing 77% m-ZrO_2 ($h \approx 7\,\mu$m) the residual strain induced shielding is, $\Delta K_d = -2.5 \pm 1$ MPa$\sqrt{m}$.

The *modulus* induced shielding depends only on K for the composite and on ϵ_s. With $\epsilon_s = 0.15$ and $\xi = 1.4$, $\bar{\mu}/\mu$ is obtained from equation (7) as, 0.4. Then, with $K \equiv K_c = 6$ MPa$\sqrt{m}$ (Fig. 1) the modulus shielding is obtained from equation (9) as $\Delta K_m = -5 \pm 2$ MPa$\sqrt{m}$.

Simple addition of the dilatational and modulus contributions would indicate toughening, $\Delta K_c \approx 7.5$ MPa$\sqrt{m}$, sufficiently large to account fully for

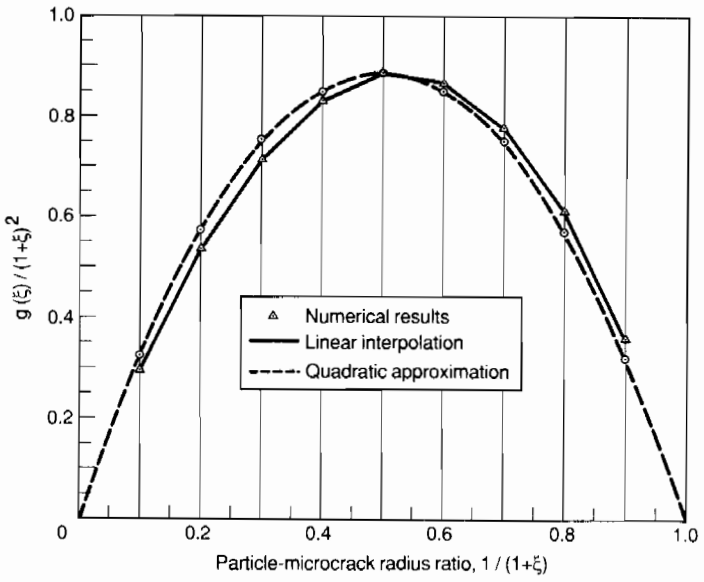

Fig. 16. Trends in the crack volume parameter g with relative crack radius ξ.

the measured toughness $K_c \approx 6\,\text{MPa}\sqrt{m}$. It should be appreciated, however, that the individual contributions to the shielding are relatively large and additivity is not strictly valid. Interaction effects must be taken into account [13] (Appendix) before more rigorous comparisons between theory and experiment are attempted. Nevertheless, the present comparison implies that the intrinsic fracture resistance of the material at the macrocrack tip, as degraded by microcracks, is appreciably smaller than the toughness of the Al_2O_3 matrix. Such behavior would be consistent with the existence of a relatively low stress near the crack plane, as noted above. More definitive assessment of degradation effects awaits computation of the interaction between the dilatational and modulus shielding for the specific microcrack geometry depicted in Fig. 12.

It is of interest to note that, for the present case, the modulus reduction and dilatational contributions to the shielding are similar in magnitude. This is important to appreciate because the former contribution cannot be readily changed, being governed almost entirely by the saturation microcrack density, ϵ_s. However, the dilatational contribution may be enhanced by increasing both the process zone size and the microcrack density within the zone. This might be achieved by superior control of the m-ZrO_2 particle size distribution which in turn, affects the nucleation of the microcracks.

5. CONCLUDING REMARKS

The present study demonstrates the importance of a close quantitative coupling between theory and experiment when attempting to interpret toughening mechanisms. In particular, the study reveals that a number of substantive problems exist in the analysis of microcrack toughening; both experimental and theoretical deficiencies are evident. Among the problems are a poor fundamental understanding of the degradation caused by the microcracks directly ahead of the crack front, limited knowledge of interactions between modulus and dilatational contributions to crack shielding, as well as experimental microcrack detectability limitations in the TEM. These topics require further study before authoritative conclusions can be reached regarding toughening in ZTA and before *ab initio* predictions of toughening trends can be contemplated.

Acknowledgement—The authors thank the Defense Advanced Research Projects Agency for financial support under Office of Naval Research contract ONR-N00014-86-K-0178.

REFERENCES

1. F. E. Buresch, *Fract. Mech. Ceram.* **4,** 835 (1975).
2. R. G. Hoagland, J. D. Embury and D. J. Green, *Scripta metall.* **9,** 907 (1975).
3. A. G. Evans, *Scripta metall.* **10,** 93 (1976).
4. A. G. Evans and K. T. Faber, *J. Am. Ceram. Soc.* **67,** 255 (1984).
5. A. G. Evans and Y. Fu, *Acta metall.* **33,** 1525 (1985).
6. J. W. Hutchinson, *Acta metall.* To be published.
7. A. G. Evans and R. M. Cannon, *Acta metall.* **34,** 761 (1986).
8. M. Rühle, N. Claussen and A. H. Heuer, *J. Am. Ceram. Soc.* **69,** 195 (1986).
9. E. E. Underwood, *Quantitative Stereology.* Addison-Wesley, Reading Mass. (1970).
10. A. H. Heuer, N. Claussen, W. M. Kriven and M. Rühle, *J. Am. Ceram. Soc.* **65,** 642 (1982).
11. D. R. Clarke, *Ultramicroscopy* **4,** 33 (1979).
12. B. Budiansky and R. J. O'Connell, *Int. J. Solid Struct.* **12,** 81 (1976).
13. P. G. Charalambides and R. M. McMeeking, *Mech. Mater.* In press.
14. I. N. Sneddon, *Proc. R. Soc.* **A187,** 229 (1946).
15. P. G. Charalambides and R. M. McMeeking. To be published.

APPENDIX: SOME MECHANICS SOLUTIONS FOR RADIAL MICROCRACKS

A1. Dilatancy

Microcracks generated around prestressed particles cause dilatancy by relief of the constraint stresses. The resulting strain experienced by an unstressed macroscopic sample containing N randomly arranged cracks per unit volume is simply N times the average volume contained within the cracks. An important aspect of this volume for microcracks around m-ZrO_2 particles in Al_2O_3/ZrO_2 is the residual crack opening that exists at the particle–matrix interface. This opening is allowed when the interface is partly decohered, as shown in Fig. 12(b). This configuration has been simplified to the model shown in Fig. 12(c) with the final constraint stress p regarded as uniform and uniaxial in the particle. The opening of such microcracks is assessed by calculation of the effect of the stress in the particle applied as a traction on the surface of a penny shaped crack.

Sneddon [14] has derived the opening of such an axisymmetrically loaded crack as

$$\delta(r) = \frac{4(1-\bar{\nu})}{\pi\bar{\mu}} \int_r^a \frac{1}{\sqrt{\alpha^2 - r^2}} \int_0^\alpha \frac{T(\rho)\rho\,\mathrm{d}\rho}{\sqrt{\alpha^2 - \rho^2}}\,\mathrm{d}\alpha \quad \text{(A1)}$$

where $T(r)$ is the traction applied to the top and bottom surfaces, $\bar{\mu}$ and $\bar{\nu}$ are the macroscopic shear modulus and Poisson's ratio for the microcracked composite material and $a = b + c$. When $T = -p$ for $0 \leqslant r \leqslant b$ and is zero otherwise, the integral (A1) gives

$$\delta(r) = -\frac{4bp(1-\bar{\nu})}{\pi\bar{\mu}} [(\xi^2 + 2\xi)^{1/2} - \xi] S\left(\frac{r}{b}; \xi\right) \quad \text{(A2)}$$

where

$$\begin{aligned} S(\rho;\xi) = {} & \{[(1+\xi)^2 - \rho^2]^{1/2} \\ & \times [1 + \xi - [(1+\xi)^2 - 1]^{1/2}]/(1+\xi) \\ & + \rho[E(1/\rho, \pi/2) - E(1/\rho, \phi)] \\ & - \rho(1 - 1/\rho^2)[F(1/\rho, \pi/2) \\ & - F(1/\rho, \phi)]\}/\{[(1+\xi)^2 - 1]^{1/2} - \xi\} \end{aligned} \quad \text{(A3)}$$

and $\phi = \sin^{-1}[\rho/(1+\xi)]$. The terms F and E are elliptic integrals of the first and second kind respectively such that

$$F(k, \phi) = \int_0^\phi \frac{\mathrm{d}\theta}{(1 - k^2 \sin^2\theta)^{1/2}} \quad \text{(A4)}$$

and

$$E(k, \phi) = \int_0^{\phi} (1 - k^2 \sin^2 \theta)^{1/2} \, d\theta. \quad \text{(A5)}$$

(It should be noted that equation (A2) corrects an error in equation (3.3.2) of Sneddon [14]). Evaluation of equation (A2) at $r = b$ gives

$$\delta_R = -4bp(1 - \bar{\nu})[(\xi^2 + 2\xi)^{1/2} - \xi]/\pi\bar{\mu}. \quad \text{(A6)}$$

(In the text the subscript R has been dropped from δ_R.) It follows from equations (A2) and (A6) that, since $S(1; \xi) = 1$, then

$$\delta(r) = \delta_R S(r/b; \xi). \quad \text{(A7)}$$

The volume within each microcrack is related to the opening by

$$\Delta V = 2\pi \int_b^{c+b} \delta(r) r \, dr \quad \text{(A8)}$$

$$= b^2 \delta_R \phi_c(\xi) \quad \text{(A9)}$$

where

$$\phi_c(\xi) = 2\pi \int_1^{1+\xi} S(\rho; \xi) \rho \, d\rho. \quad \text{(A10)}$$

The integral in equation (A10) has been evaluated numerically and the results shown in Fig. 16. The function $\phi_c(\xi)$ can be approximated by

$$\phi_c(\xi) \equiv \xi^3 g(\xi) = 3.56\xi \quad \text{(A11)}$$

and the comparison with the numerical results is shown in Fig. 16. The approximation (A11) is used in equation (5) in the text.

A2. Modulus reduction

The self-consistent method may be used to estimate the change in the macroscopic elastic moduli caused by microcracks. This method requires the calculation of the strain energy increment due to the introduction of the microcracks, in the absence of constraint stresses, but in the presence of applied stress. As before, the simplified model illustrated in Fig. 12(c) is used. The applied stress is considered to be hydrostatic and the bulk modulus calculated, leading to an estimate of the shear modulus. The strain energy can be computed by first evaluating the microcrack opening.

The opening caused by the applied stress σ acting on a penny shaped microcrack is [14],

$$\delta_1(r) = 4\sigma(1 - \bar{\nu})[(b + c)^2 - r^2]^{1/2}/\pi\bar{\mu}. \quad \text{(A12)}$$

This opening tendency induces a tension in the particle, σ_p, modelled as uniform. The contribution to the opening due to σ_p for $r \geq b$ is given directly by equation (A2) with p replaced by σ_p. The resultant microcrack opening is obtained by summing equations (A2) and (A12). At $r = b$, the net opening is

$$\delta^*/b = 4(1 - \bar{\nu})[(\sigma - \sigma_p)(\xi^2 + 2\xi)^{1/2} + \sigma_p \xi]/\pi\bar{\mu}. \quad \text{(A13)}$$

Given that the strain in the particle is approximately $\delta^*/2d$ [where d is the interface crack length, Fig. 12(c)], the uniaxial stress in the inclusion can be related to the opening by

$$\sigma_p = E_p \delta^*/2d \quad \text{(A14)}$$

where E_p is Young's modulus for the particle. Thus δ^* can be eliminated between equation (A13) and (A14) to give an explicit expression for the stress

$$\sigma_p = \frac{(\xi^2 + 2\xi)^{1/2}\sigma}{\pi\bar{\mu}d/2(1 - \bar{\nu})E_p b + (\xi^2 + 2\xi)^{1/2} - \xi}. \quad \text{(A15)}$$

The resulting combination of equations (A2) and (A12) gives the required relation for the opening

$$\delta(r) = \frac{4\sigma(1 - \bar{\nu})b}{\pi\bar{\mu}} \left\{ [(1 + \xi)^2 - (r/b)^2]^{1/2} - \frac{(\xi^2 + 2\xi)^{1/2} S(r/b; \xi)[(\xi^2 + 2\xi)^{1/2} - \xi]}{\pi\bar{\mu}d/2(1 - \bar{\nu})E_p b + (\xi^2 + 2\xi)^{1/2} - \xi} \right\}. \quad \text{(A16)}$$

The microcrack opening is related to the strain energy removed from the system by reversible microcrack formation, U, as

$$U \equiv \sigma\pi \int_b^{b+c} r\delta(r) \, dr$$

$$= \frac{2\sigma^2(1 - \bar{\nu})b(\xi^2 + 2\xi)^{1/2}}{3\pi\bar{\mu}} \left\{ 2\pi(\xi^2 + 2\xi) - \frac{3\phi_c(\xi)[(\xi^2 + 2\xi)^{1/2} - \xi]}{\pi\bar{\mu}d/2(1 - \bar{\nu})E_p b + (\xi^2 + 2\xi)^{1/2} - \xi} \right\}. \quad \text{(A17)}$$

The self-consistent model [12] requires that the strain energy in the microcracked body be the sum of that stored in the uncracked material and that removed from the system by the reversible formation of the microcracks at a fixed macroscopic stress. Consequently for N identical isotropically arranged microcracks per unit volume

$$\sigma^2/2\bar{B} = \sigma^2/2B + NU \quad \text{(A18)}$$

where B is the bulk modulus of the uncracked material and $\bar{B}$ is the effective bulk modulus of the microcracked material. The above result contains the unknowns, $\bar{B}$, $\bar{\nu}$, and $\bar{\mu} = 3\bar{B}(1 - 2\bar{\nu})/2(1 + \bar{\nu})$. However, with the simplification, $\nu \equiv \bar{\nu} \approx 0$, the shear modulus can be explicitly derived as

$$\frac{\bar{\mu}}{\mu} \approx 1 - \frac{16\epsilon(1 + 2\xi^{-1})^{3/2}}{9} \left\{ 1 - \frac{1.70[(\xi^2 + 2\xi)^{1/2} - \xi]/(\xi + 2)}{\pi\bar{\mu}d/4\mu_p b + [(\xi^2 + 2\xi)^{1/2} - \xi]} \right\}. \quad \text{(A19)}$$

Some confidence in this simplified result can be gained by examining the limit $\xi \to \infty$, representing microcracks with very small central inclusions. Specifically equation (A19) gives, $\bar{\mu}/\mu = 1 - 16\epsilon/9$, which approximates well the exact result for penny shaped microcracks [12]. Trends in the shear modulus have been computed from equation (A19) for selected values of ϵ, ξ and $\mu_p b/\mu d$ (Table A1).

For present purposes, an estimate of d needed to obtain $\bar{\mu}/\mu$ from Table A1, can be deduced from the measurements of residual microcrack opening. This opening must be produced by a combination of transformation and thermal strains, such that the traction p [Fig. 12(c)] is

$$p \approx E_p(\delta_R/2d - \theta^T) \quad \text{(A20)}$$

where θ^T is the net unconstrained misfit strain normal to the microcracks. This expression for p can be inserted into equation (A6) to give

$$\frac{b}{d} = \frac{2\theta^T b}{\delta_R} - \frac{\pi\bar{\mu}}{2(1 - \bar{\nu})E_p[(\xi^2 + 2\xi)^{1/2} - \xi]} \quad \text{(A21)}$$

with $\theta^T \sim 0.019$, $\delta/b \sim 0.03$, $\mu/\bar{\mu} \sim 1$ and $\xi = 1.4$, $d/b \sim 1.5$. The interface crack is thus predicted to extend substantially along the particle–matrix interface. Such behaviour is seemingly consistent with the observations of interface cracking (Fig. 7).

Incorporating this value for d/b into equation (A19) indicates that for $\xi \approx 1.4$

$$\bar{\mu}/\mu \approx 1 - 5.8\epsilon + 8\epsilon^2 \quad \text{(A22)}$$

as noted in the text.

Table A1. Relative modulus of a material microcracked with radial cracks of length c around particles of radius $b(\xi = c/b)$ with interface debonds of length d

(i) $\xi = 1.4$

	$\bar{\mu}/\mu$			
ϵ	$b\mu_p/d\mu = 0.1$	$b\mu_p/d\mu = 0.5$	$b\mu_p/d\mu = 1.0$	$b\mu_p/d\mu = 10$
0.05	0.69	0.73	0.76	0.82
0.10	0.40	0.50	0.55	0.54
0.15	0.17	0.30	0.33	0.47
0.20	0.06	0.16	0.21	0.31
0.25	0.02	0.06	0.09	0.15

(ii) $b\mu_p/d\mu = 0.5$

	$\bar{\mu}/\mu$				
ϵ	$\xi = 0.5$	$\xi = 1.0$	$\xi = 1.5$	$\xi = 2.0$	$\xi = 10$
0.05	0.36	0.65	0.75	0.79	0.89
0.10	0.10	0.37	0.52	0.60	0.78
0.15	0.01	0.18	0.33	0.42	0.67
0.20	—	0.07	0.18	0.28	0.52
0.25	—	—	0.08	0.16	0.46

The shear modulus of the particle is μ_p, of the uncracked material is μ and with microcracks is $\bar{\mu}$. The microcrack density ϵ is Nc^3, where N is the number of microcracks per unit volume.

Table A2. Combined dilatation and modulus reduction [13, 15]

		$\Delta K/K$	
$\bar{\mu}/\mu$	$\theta^T\sqrt{hE}/K_c$	Summation	Interaction
0.34	0.06	0.59	0.77
0.14	0.08	0.74	0.9

A3. The toughening

In the text, the toughening effect contributed by the dilatation and modulus reduction have been treated separately and the results added to provide an estimate of the combined effect. This procedure gives a result which is correct to lowest order and is valid when the shielding is small compared with the stress intensity associated with the applied loads. Numerical results obtained by Charalambides and McMeeking [13, 15] for combined dilatation and modulus reduction can be used to provide an indication of the validity of this approach for the present case (Table A2). It is apparent that the additive procedure is inadequate when large modulus reduction effects are present. Further studies of such interaction effects are needed to fully interpret microcrack toughness in ZTA.